Nanoscale

CuS Nanoparticles in Humid Environments: Adsorbed Water Enhances the Transformation of CuS to $CuSO_4$

Journal:	*Nanoscale*
Manuscript ID	NR-ART-08-2020-005934.R1
Article Type:	Paper
Date Submitted by the Author:	19-Aug-2020
Complete List of Authors:	Wu, Haibin; University of California San Diego, Department of Chemistry and Biocheistry Or, Victor; University of California San Diego, Chemistry and Biochemistry Calzada, Sabrina; University of California San Diego Grassian, Vicki; University of California San Diego,

CuS Nanoparticles in Humid Environments: Adsorbed Water Enhances the Transformation of CuS to $CuSO_4$

Haibin Wu,[1] Victor Or,[1] Sabrina Gonzalez-Calzada,[2] Vicki H. Grassian[1,2,3]*

[1]Department of Chemistry & Biochemistry, University of California San Diego, La Jolla, CA 92093, United States

[2]Departments of Nanoengineering, University of California San Diego, La Jolla, CA 92093, United States

[3]Scripps Institution of Oceanography, University of California San Diego, La Jolla, CA 92093, United States

*To whom correspondence should be addressed: vhgrassian@ucsd.edu

Abstract

Covellite copper sulfide nanoparticles (CuS NPs) have attracted immense research interest due to their widespread use in a range of biological and energy applications. As such, it is crucial to understand transformations of these nanomaterials and how these transformations influence the behavior of these nanoparticles in environmental and biological systems. This study specifically focuses on understanding the role of water vapor and adsorbed water in the transformation of CuS NP surfaces to $CuSO_4$ in humid environments. Surface sulfide ions are oxidized to sulfate by oxygen in the presence of water vapor, as detected by atomic force microscopy infrared spectroscopy (AFM-IR) and in-situ attenuated total reflectance Fourier transform infrared spectroscopy (ATR-FTIR). These results show that the transformation of CuS to $CuSO_4$ is highly dependent on relative humidity (RH). Sulfide to sulfate conversion is not observed to any great extent at low RH (< 20%) whereas there is significant conversion at higher RH (> 80%). X-ray photoelectron spectroscopy (XPS) analysis confirms that sulfide is irreversibly oxidized to sulfate. Furthermore, it shows that initially Cu ions possess the original oxidation state as the original covellite, i.e. Cu^+, but then these are oxidized to Cu^{2+} at higher RH. The formation of $CuSO_4$ has also been confirmed by HRTEM. These analyses show that adsorbed water on the NP surfaces enhances the conversion of sulfide to sulfate and the oxidation of Cu^+ to Cu^{2+} in the presence of molecular oxygen.

Introduction

With the rapid development of nanotechnology in the past decades, nanomaterials have been widely applied in many aspects, e.g. catalysts, cosmic products, drug delivery media, sensor or electrode materials.[1-4] Among various types of nanomaterials, copper sulfide nanomaterials have been attracting research attention due to its unique properties and applications in chemical sensors and catalysis.[2, 5-7] Copper sulfide represents a family of chemical compounds including two prominent forms: chalcocite (Cu_2S) and covellite (CuS). Covellite is known as the relatively more stable structure when exposed to oxidizing conditions at atmospheric pressure.[8] Additionally, covellite nanoparticles (NP) have tunable localized surface plasmon resonances (LSPR) in the near-infrared region.[9] Therefore, in addition to the applications as sensor and electrode materials, covellite NPs have received significant attention as a potential material for imaging and photothermal therapies.[10-12]

Although the toxicity of covellite NPs is limited by its low solubility in water,[13, 14] given the wide biological and catalytic applications, these NPs experience an array of different reactive conditions, such as within biological organisms and/or release into the environment which can impact is solubility through the adsorption of chelating ligands and surface transformations. Thus, there are concerns about potential toxicity generated from surface transformations of covellite NPs.

Water vapor has been reported to be reactive with some semiconductors by promoting surface oxidation, such as NiS.[15] However, few studies directly address covellite NP oxidation in presence of molecular oxygen and water vapor. Herein, we investigated surface transformations of covellite NPs at different RHs. These transformations were

observed through *ex-situ* (AFM-IR spectroscopy and XPS) and *in-situ* methods (ATR-FTIR spectroscopy) as a function of relative humidity (RH). The results indicate these transformations are promoted in the presence of water, forming $CuSO_4$ at high RH levels. The physiochemical properties of CuS NPs are highly dependent on the surface states coatings.[16-20] Thus, formation of a $CuSO_4$ surface layer can alter the physiochemical properties of the nanoparticle, e.g. it can lead to increased solubility and enhanced ion dissolution as well as decrease in its LSPR performance[17]. As reported in previous studies, Cu ions are cytotoxins, able to damage DNA and proteins.[21-25] As such, transformations of CuS nanoparticle surfaces have a range of potential consequences from its use in different applications to its toxicity.

Experimental Details

Synthesis of Covellite Nanoparticles. CuS nanoparticles were synthesized in this study in the absence of any surfactants so as to have exposed CuS at the surface for these surface transformation studies. The procedure followed involved mixing 0.456g copper (II) nitrate • hexahydrate (Sigma Aldrich), 0.6 g thiourea (Acros Organics), and 20mL of ethylene glycol (Fisher Scientific) in a 50 mL three neck flask. The system is under initial vacuum and then nitrogen gas is introduced to minimize exposure to air. The temperature was raised to 110 ºC and kept for ten minutes. A mixture of 5mL of 1M sodium hydroxide and 5 mL ethylene glycol was injected into the flask. The solution was then held for an additional five minutes before cooling down to room temperature. The CuS NPs were separated by centrifuging for 10 mins at 10,000 rpm. The NPs were washed four times by water quickly to remove the excessive ions and precursors. The as-synthesized CuS NPs were immediately transferred a vacuum desiccator to avoid potential further oxidation by air.

CuS Nanoparticle Characterization The crystalline lattice was analyzed by powder X-ray diffraction (PXRD). XRD was performed on a Bruker AXS D8 FOCUS diffractometer equipped with Cu-K radiation (λ = 1.54180 Å). The low-resolution transmission electron microscopy images were obtained by using TECNAI G2 SPHERA transmission electron microscopy (TEM) operated at 80 kV. High-resolution TEM (HRTEM) images were carried out on a JEOL JEM-2800 (HR) electron microscope operated at 200 kV.

AFM-PTIR Spectroscopy Samples were analyzed using a nanoIR2 (Anasys Instruments - Bruker, Santa Barbara, CA) microscopy system equipped with a tunable mid-IR optical parametric oscillator laser (OPO). AFM imaging of conducted under ambient conditions at 298 K and a RH of ~40% at ambient pressure. Images were collected at a scan rate of 0.5 Hz using gold-coated silicon nitride probes (tip radius ⩽ 30 nm) 0.07 – 0.4 N m^{-1} spring constant and 13 ± 4 kHz resonant frequency in contact mode. Photothermal infrared (PTIR) spectra were collected at different locations across the surface with a nominal spatial resolution of < 30 nm, a spectral resolution of 8 cm^{-1}, co-averaging 128 laser pulses per wavenumber. All spectra shown are taken on a single point with no smoothing filters applied. Background corrections were done by substrate subtraction using a spectrum taken on the bare gold roughly 100 nm away. Chemical maps were taken by keeping the laser at a fixed wavelength, with a scan rate of 0.1 Hz, averaging 8 times per pixel.

X-ray photoelectron spectroscopy X-ray photoelectron spectroscopy (XPS) measurements were performed by using an AXIS Supra by Kratos Analytical. The binding energy was calibrated against adventitious carbon 1s peak at 284.5 eV.

ATR-FTIR spectroscopy ATR-FTIR spectra were recorded using a 500 µl horizontal ATR flow cell with an AMTIR element (Pike Technologies Inc.). A Nicolet 6700 FTIR spectrometer equipped with an MCT-A detector was used. Each spectrum was collected with 264 scans at an instrument resolution of 4 cm^{-1} in the AMTIR spectral range (750 to 4000 cm^{-1}). CuS NPs, 3 mg, were dispersed in 1 mL methanol and dropped on the AMTIR element. The slurry was dried in a nitrogen atmosphere overnight.

Results and Discussion

Characterization of CuS Nanoparticles

The morphology of the as-synthesized NPs was characterized by TEM. The NPs are seen to be aggregated as shown in Figure 1a with individual particles sizes mostly below 20 nm with a peak in the size distribution of 8 nm. The particles are aggregated because there was no purposeful surfactant added to the synthesis so as to investigate CuS NP surface transformations. The crystalline structure of the CuS NPs is analyzed by PXRD, as shown in Figure 1c. The standard data for covellite (JCPDS no. 06-0464) is also shown as blue bars in Figure 1c for comparison. The diffraction peaks are indexed to different planes: (101), (102), (103), (006), (106), (110), (108) and (116) plane. All of these different planes agree well with the standard data assigned to covellite phase. The overlapped peaks (103) and (006) are weaker than the (110) peaks suggests that preferential growth of CuS NPs is along with <110> directions, also indicating polysulfide in CuS.[26]

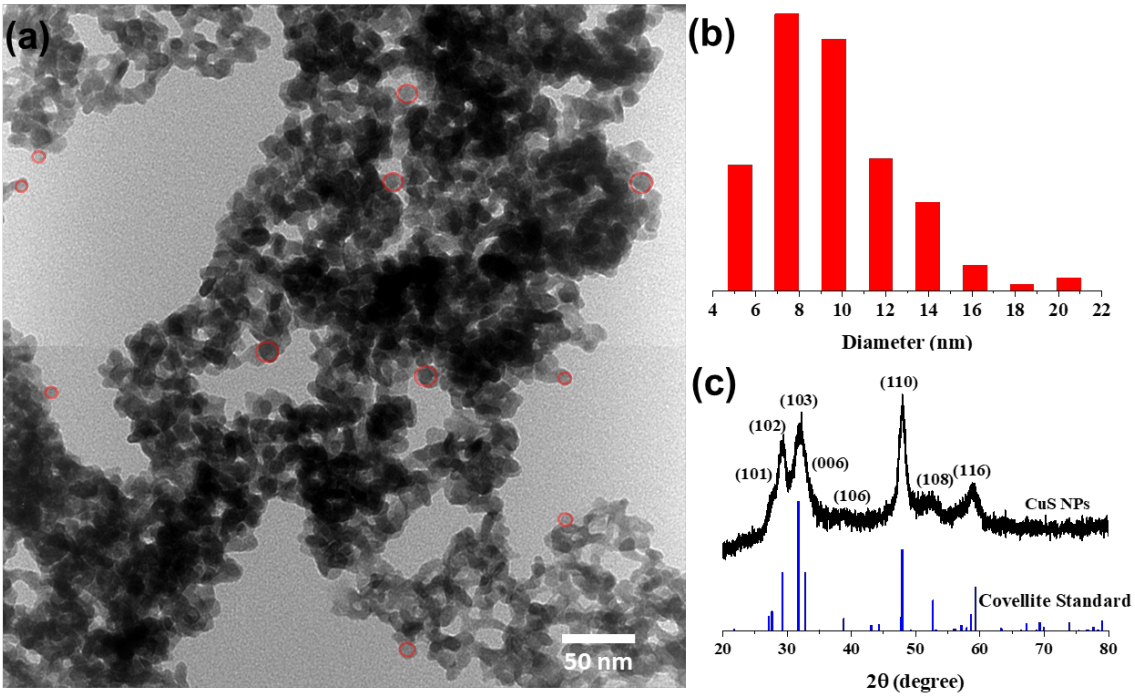

Figure 1. (a) TEM image of the as-synthesized covellite nanoparticles. (b) Size distribution of the individual nanoparticles within the observed aggregates were determined by measuring the diameter of distinct particles which were typically at the edge of the larger aggregate (e.g. see red circles within the image). (c) powder X-ray diffraction data of as-synthesized covellite NPs to standard diffraction data for the covellite phase.

ATR-FTIR Spectroscopy

The ATR–FTIR spectra shown in Figure 2 provides evidence for surface transformations and oxidation by monitoring the appearance of new vibrational bands as the CuS nanoparticles are exposed to oxygen at different RHs. The oxidation product of interest is SO_4^{2-} which displays vibrational frequencies in the spectral range from around 900 to 1100 cm^{-1}, as labeled in Figure 2. As shown in these spectra, the peaks in this region do not become apparent at low RH 2%, but do show up at RH 39 and 87%. The fundamental vibration frequencies of an isolated sulfate ion, SO_4^{2-}, with T_d symmetry, is around 971–993 and 1070 –1190 cm^{-1} for the symmetric stretching and asymmetric stretching modes, respectively.[27-29] The surface oxidized spectra are more complicated that simple isolated

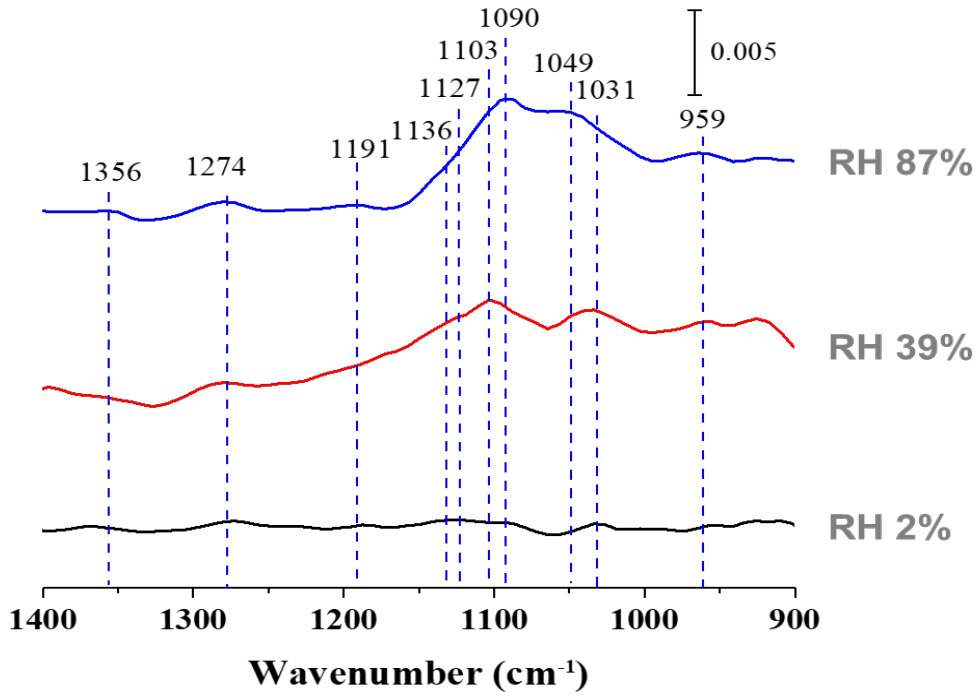

Figure 2. ATR-FTIR spectra of oxidized covellite after 2 hrs. at RH 2%, RH 39% and RH 87%, respectively.

sulfate ion due to various interactions with the surface leading to both a decrease in symmetry of the ion and different bonding mode coordinations to the surface. [27, 30] Previous literatures proposed sulfate may interact with a surface i.e. hematite or fluorite by forming inter-sphere complex with surface cations, which display the C_{3v} (monodentate with three absorption bands) and C_{2v} (bidentate with four absorption bands) symmetry. [27, 30] Thus the peaks in this region are consistent with the formation of sulfate. For example, a broad peak centered around 959 cm^{-1} appearing at high RH values is assigned to symmetric stretching vibration for adsorbed species. The lower value for the symmetric stretching than the isolated ion suggests that sulfate may interact with water or OH^- and Cu ions on the surface (i.e. S–O ••• OH/H_2O ••• Cu^+) that is similar the interaction found in $Cu_x(OH)_ySO_4$ compounds.[29, 30] The asymmetric stretching of S–O shows multiple peaks depending on the coordination environment. Peaks near at 1049, 1136, and 1191 cm^{-1} may be assigned to a bidentate complex, and the bands at 1031 and 1127 cm^{-1} to a monodentate complex.[28,

[30, 31] A previous study about on adsorbed sulfate has suggested that the peak at 1360 cm^{-1} might be caused by the formation of polysulfate on the surface.[30] Additionally, the peak at 1274 cm^{-1} may reflect the formation of an adsorbed sulfate–water complex.[30, 32] In order to determine if adsorbed water may cause the oxidation of sulfide, a control experiment was carried out under a nitrogen atmosphere. The comparison suggests that molecular oxygen acts as the oxidant but not water in the oxidation process.

The time dependence of the surface oxidation process was observed *in-situ* by ATR–FTIR spectroscopy as shown in Figure 3. At low RH, 2%, there is little change in the vibrational spectra. However, the intensity of sulfate peaks increases with oxidation time at higher RHs. The integrated peak areas from 1050 to 1170 cm^{-1} are plotted as a

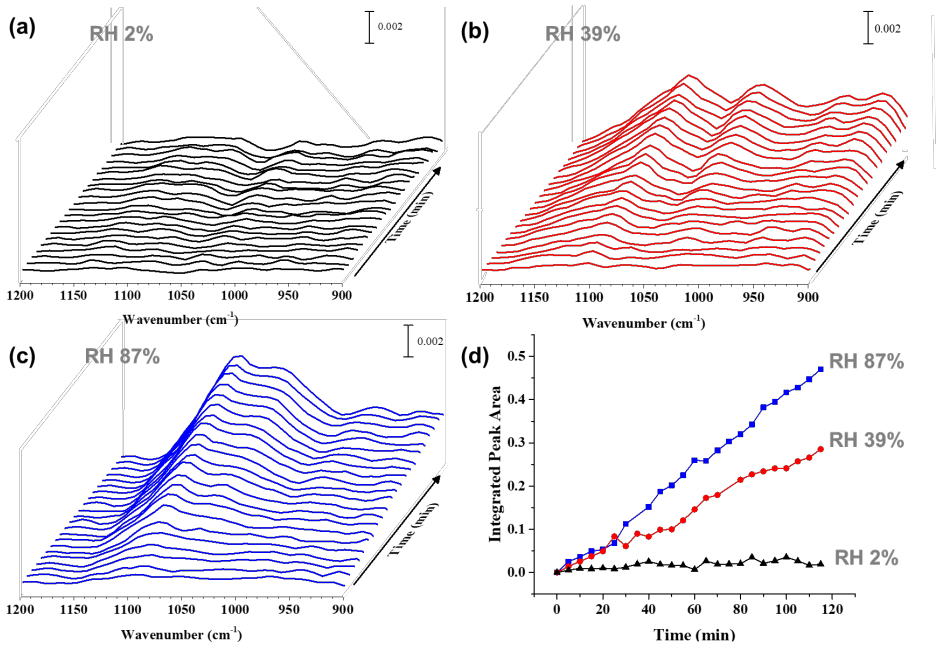

Figure 3. (a) (b) (c) ATR-FTIR spectra of CuS under ambient conditions as a function of time at different RH: 2%, 39% and 87%, respectively. (d) Integrated peak area of sulfate absorption bands (1050 to 1170 cm^{-1}). Each spectrum was recorded every five minutes for a total time of 120 minutes.

function of time at the different RH. These data show that the rate of sulfate formation is ca. 1.5 times faster at 87% versus 39% RH whereas there is little formation at 2% RH.

In order to better understand the interaction of water with the surface, the spectral region from 2600 to 3500 cm^{-1} was monitored during reaction at 87% RH as shown in Figure 4. As the time proceeds, a very broad band appears in the spectra. It is interesting that the strongest broad peak is at low wavenumbers that that typically found for the O–H stretch of adsorbed water. However, reports of low frequency bands even as low as 2980 cm^{-1} have been attributed to O–H stretching mode of $Cu(H_2O)_n^+$, indicating that water molecules bond to surface Cu ions.[33] In addition, there is a broad peak around 3350 cm^{-1}

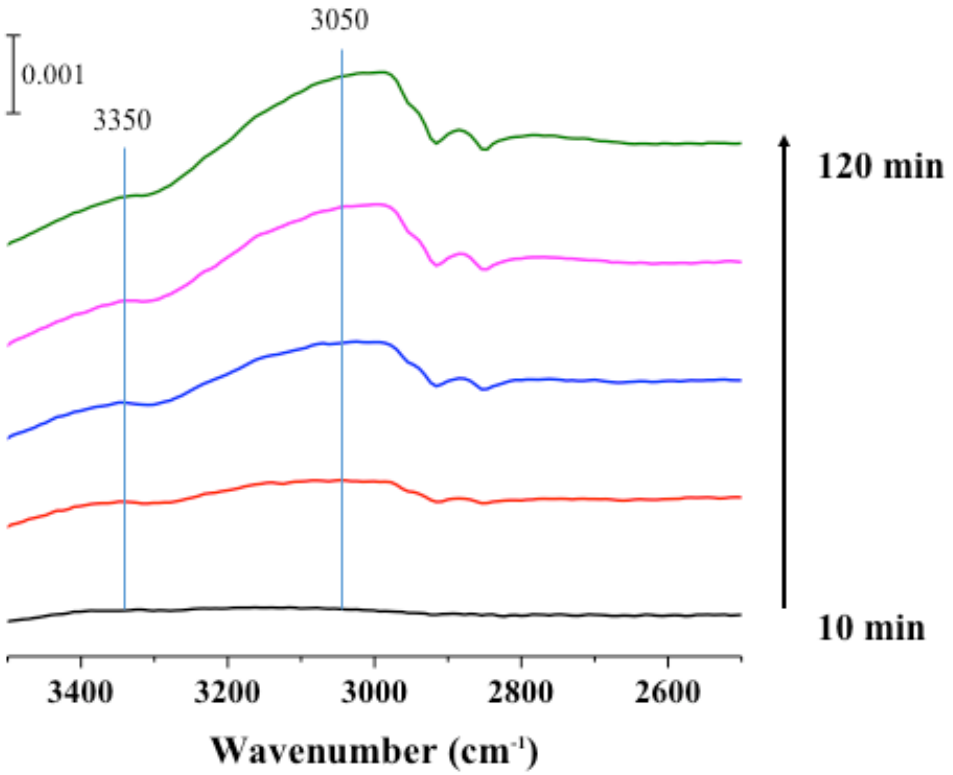

Figure 4. ATR-FTIR spectra in the spectral region extending from 2500 to 3600 cm^{-1} as a function of time following. This is the same experiment shown in Figure 3c but for a different spectral region. It can be seen that as the surface transforms a broad peak grows in during at RH 87% in this higher wavenumber region. This is associated with adsorbed water on the surface.

which is closer in frequency to the O–H stretching vibration of water molecules not directly bonded to surface metal ions but instead interacting with the surface and other adsorbed water through hydrogen bonding interactions. Overall, these data suggest that water adsorbs on the surface and participates in the oxidation of sulfide to sulfate. This transformation is irreversible as the sulfate peaks do not decrease over time in the absence of oxygen and relative humidity. Our results are in agreement with the previous simulation that the adsorption and oxidation of iron sulfide surfaces can be enhanced due to adsorbed water.[34]

X-Ray Photoelectron Spectroscopy in Cu 2p and S 2p Regions

Further evidence and additional insights of the transformation of these CuS nanoparticle surfaces are provided by XPS. A study by Evans Jr. *et al*. indicates that covellite has an unique crystalline structure of hexagonal close-packing: Cu atoms occupy two different sites - tetrahedral and triangular coordination; S atoms form disulfide groups and single sulfide ions, as shown in Figure 5a.[35] Cu_3S and CuS_3 layers resemble through disulfide bridge. The valence of Cu and S in covellite has been the subject of debate for several years.[18, 36-41] Covellite is normally described as mixed valance state of Cu and S. Previous studies proposed that the appropriate oxidation formalism for CuS is proposed to be $(Cu^+)_3S^{2-}(S_2)^-$, in which oxidation state of Cu in covellite CuS is Cu^+ rather than Cu^{2+} and S has various valences such S^{2-} and S_2^-.[36, 37] However, other studies carried by ^{63}Cu NMR indicates Cu possesses mixed valence states with Cu^+ and Cu^{2+}.[39, 42-44] Furthermore, simulations have propose a structure with no integer valences for the copper ions.[45] Here we employ X-ray photoelectron spectroscopy to analyze the surface chemical states of covellite NPs. Figure 5b depicts the Cu 2p and S 2p regional XPS spectra of the freshly

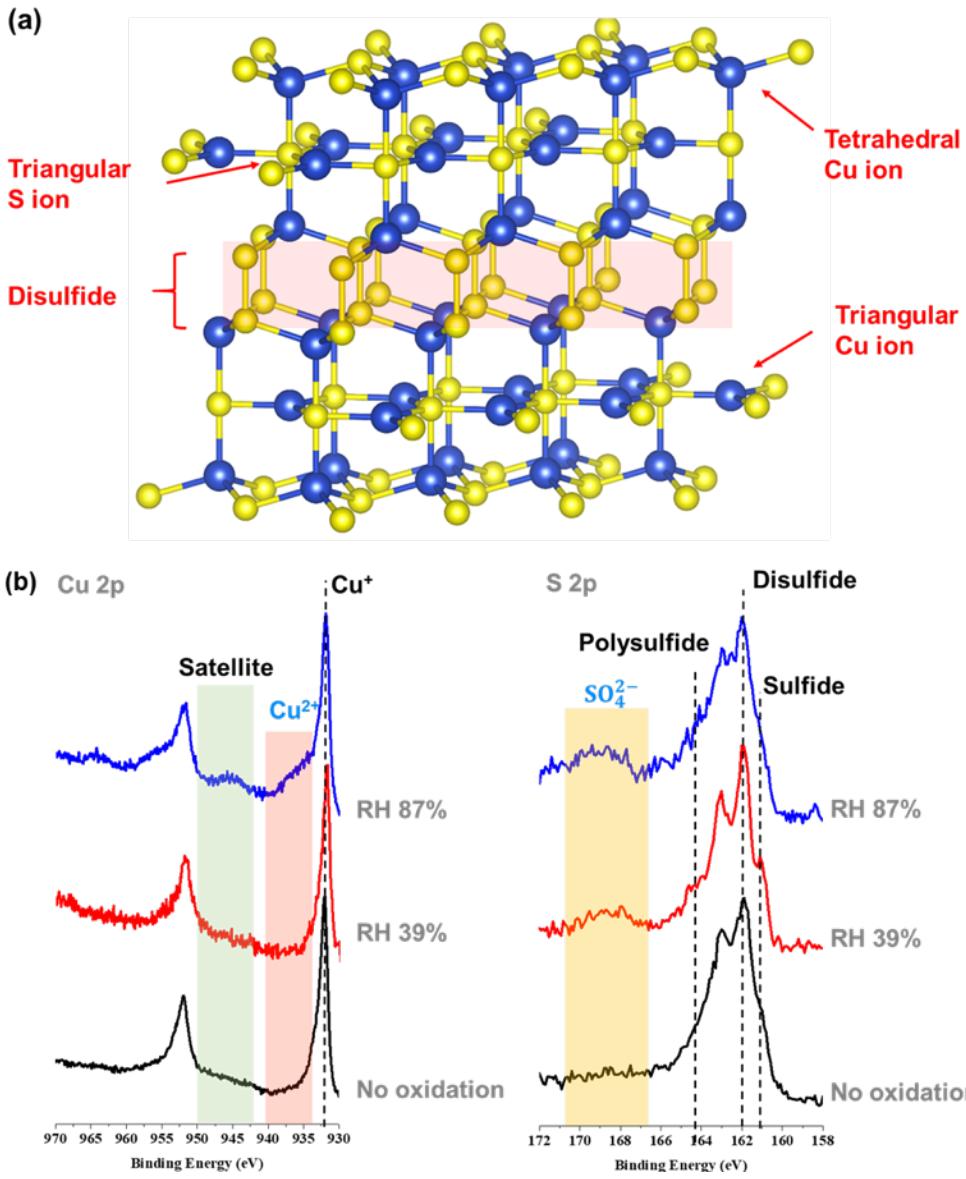

Figure 5. (a) crystal model of covellite, (b) High-resolution XPS characterization of covellite samples under various condition: Cu 2p region (left) and S 2p region (right). The blue spheres represent Cu and the yellow spheres represent sulfur. The binding models are visualized by VESTA.

synthesized covellite NPs under different conditions. According to XPS results shown in Figure 5b, the freshly synthesized covellite NPs do not show noticeable oxidation even though sample transfer process exposed to room air for a short time. In contrast, the samples exposed to pure oxygen in presence of water vapor display sulfide oxidation as evident by sulfate at 168 eV in the S 2p region.[46] The peaks at 161.8 and 163.0 eV are

regarded as S 2p1/2 in sulfide compounds,[47] and the other peak of S at 164.2 eV is very close to polysulfide 2p1/2 in chalcogenides caused by high Cu-deficiency in the near surface region.[18, 26, 48, 49] The XPS in the Cu 2p region displays two intense doublet peaks at 932.0 and 951.9 that are assigned to 2p3/2 and 2p1/2 consistent with Cu in covellite, respectively.[36] As shown in Figure 5b, Cu peaks at 932.0 eV have asymmetric tails which is caused by kinetic energy losses in the interaction of photoelectrons with free charge carriers and is no evidence for Cu^{2+} as described previously. [18] It is also important to note that shake-up satellite peaks at around 945 and 965 eV originating from Cu (II) [50, 51] are not observed in XPS spectra for freshly synthesized sample and sample oxidized at RH 39%, indicating Cu^{+} is the main format in covellite NPs instead of Cu^{2+}.[4, 52] For the sample, oxidized at RH 87%, the Cu 2p spectrum indicates a peak showing around 936 eV for the compound of $CuSO_4$ as labeled in the Figure 5b, while this is not noticeable for the freshly synthesized sample, the sample oxidized under RH 39% does show evidence for Cu^{2+}. It is evident that at high RH surface copper ions in covellite are also oxidized and the product that forms is $CuSO_4$, however at lower relative humidity, RH 39%, the formation of an unusual Cu_2SO_4 surface species is suggested, possibly an intermediate prior to formation of $CuSO_4$ that is seen for higher RH.

Imaging Techniques: Atomic Force Microscopy Coupled to Infrared Spectroscopy and High-Resolution Transmission Electron Microscopy

Additional insights into the transformation of nanoparticles can be obtained through imaging techniques. Figure 6 shows the PTIR spectra and the corresponding AFM image of the 87% RH oxidized CuS NPs deposited on a gold substrate utilizing AFM-PTIR spectroscopy. Individual NPs are expected to be ca. 8 nm in diameters, and the AFM

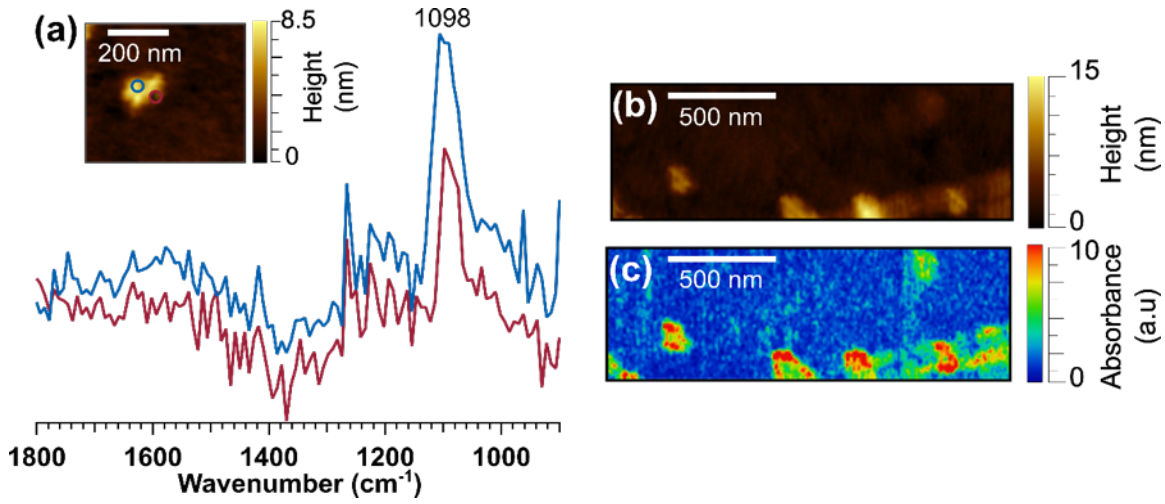

Figure 6. (a) PTIR spectroscopy for particles, with an inset showing the corresponding AFM height image of oxidized covellite NPs exposed to pure oxygen for 24 hrs at RH 87% with height images. (b) AFM height image and (c) chemical map of the sulfate rich regions of the particle taken at 1098 cm^{-1}.

spectra show that the nanoparticles remain highly aggregated when deposited onto the surface but mostly in two dimensions, x-y plane not in the z-direction which is a measurement of the height. PTIR spectra taken on the center and edge of a particle show a single peak at 1098 cm^{-1}. As both CuS and the underlying gold substrate do not have any vibrational modes in the mid-infrared spectral region, this peak can be attributed to the $\nu_{as}(SO_4^{2-})$ from oxidation of the CuS NPs. Although AFM-IR is not a surface selective technique, we expect the aggregates to contain the oxidized material, and subsequently provide enough sulfate ions for signal detection. Chemical mapping taken of the 1098 cm^{-1} peak shows the spatial distribution of the sulfate groups, which is highest at the center of the aggregate. The presence of these sulfate modes provides further evidence that these sulfate containing NPs are formed irreversibly under elevated humidity.

In order to further confirm the formation of $CuSO_4$ at high RH, the reacted sample was imaged by HRTEM. Figure 7a shows the HRTEM image of the oxidized sample at

RH 87%. The corresponding FFT pattern of HRTEM fringes also indicate with two distinct crystal phases. The d-spacing values are 0.197 nm and 0.320 nm, respectively. The former one is very close to the value for crystal facet (320) of $CuSO_4$ (PDF 15-0775) and the latter

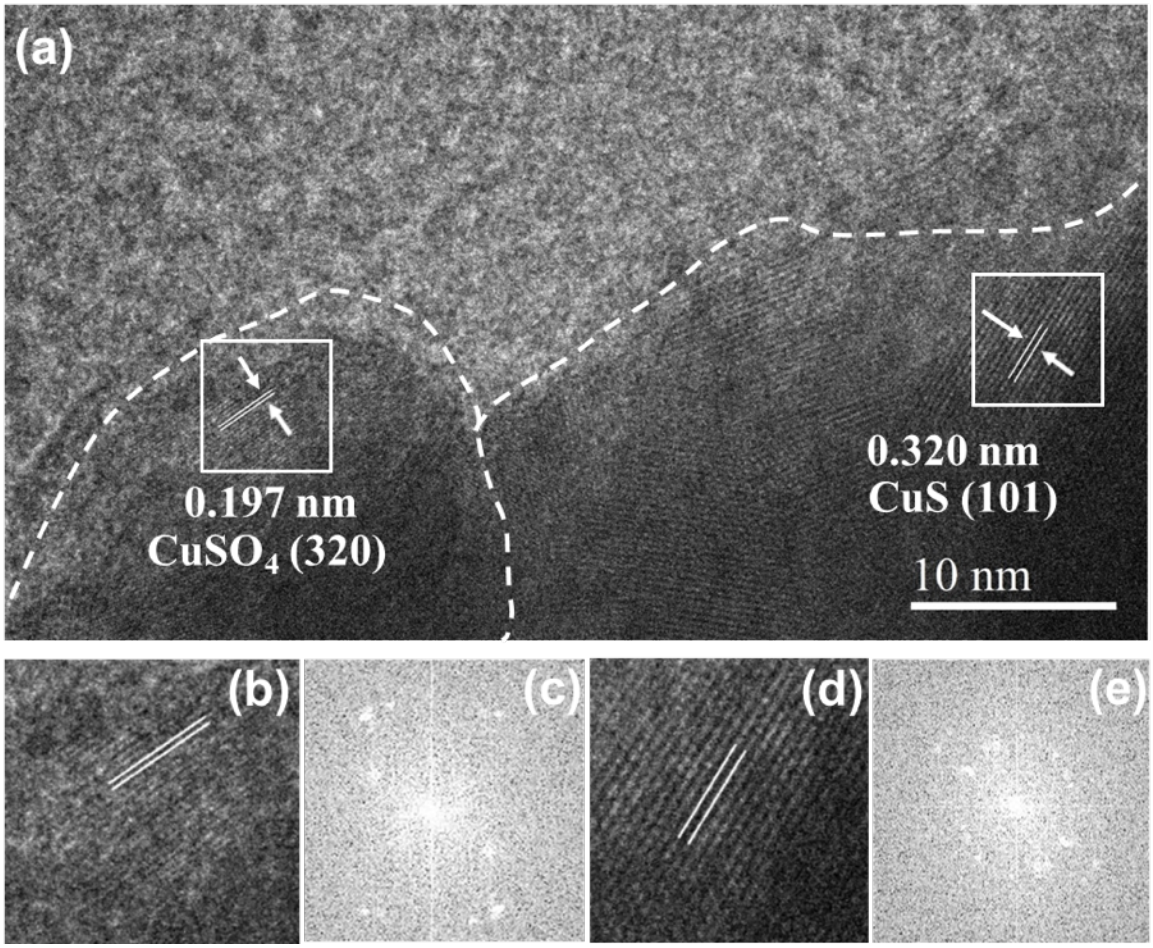

Figure 7. (a) High resolution TEM image of covellite NPs after oxidation at RH 87%, (b) the selected $CuSO_4$ phase, (c) the FFT pattern of the selected $CuSO_4$ phase, (d) the selected CuS phase, (e) the FFT pattern of the selected CuS phase.

is for (101) of covellite (PDF 15-0775). Therefore, the new features rather than CuS is likely caused by the formation of $CuSO_4$.

Surface Transformations and Oxidation of CuS in Humid Environments

Surface transformations of CuS, covellite, NPs are shown in humid environments when exposed to air. Simulations show that oxygen preferentially adsorbs onto sulfide

surfaces compared to water[53] with molecular oxygen reversibly adsorbing onto covellite NP surfaces when covered by organic surfactants (e.g. oleylamine).[17] In the absence of an organic surfactant, molecular oxygen reacts with sulfide at the surface to form sulfate as seen here. In addition to sulfide oxidation, oxygen can also chemically bond to the copper ion center on the sulfide surface.[34, 53] Oxygen acts as an electron acceptor and able to oxidize both Cu^+ and sulfide ions. Furthermore, the reduced oxygen ion is reported to generate reactive oxygen species with the help from Cu^+.[54] Therefore, several different reactions may be involved in the formation of Cu^{2+} and SO_4^{2-} and the transformation of CuS in humid environments. These include:

$$H_2O \rightarrow H^+ + OH^- \quad (1)$$

$$H_2O + S^{2-} \rightarrow HS^- + OH^- \quad (2)$$

$$O_2 + 2HS^- \rightarrow H_2O_2 + S_2^{2-} \quad (3)$$

$$O_2 + Cu^+ \rightarrow O_2^- + Cu^{2+} \quad (4)$$

$$O_2^- + 2H^+ + Cu^+ \rightarrow H_2O_2 + Cu^{2+} \quad (5)$$

$$H_2O(ad) + Cu^{2+} \rightarrow H^+(ad) + OH^{\bullet}(ad) + Cu^+ \quad (6)$$

$$2OH^{\bullet}(ad) \rightarrow H_2O_2 \quad (7)$$

$$H_2O_2 + 2S^{2-}/S_2^{2-} \rightarrow 4H_2O + SO_4^{2-} \quad (8)$$

Several important features can be gleaned from the proposed various steps that may be involved. First, there is the formation of reactive oxygen species (ROS) including superoxide, hydroxyl free radical and hydrogen peroxide. The ROS can further oxidize sulfide and disulfide to sulfate. Second, ROS in can reacts with protons from water

molecules to yield Cu^{2+} and hydrogen peroxide. Thus, in a dry environment, the oxidation process is inhibited resulting in little transformation of the sulfide surface. It is interesting that the adsorption of water is enhanced on the oxidized surface as seen in the infrared spectra. This indicates an increase in the adsorption energy of water as the transformation proceeds..[34]

A simplified depiction of the transformation of CuS NPs under different RHs are summarized in Figure 8. As depicted in Figure 8, the covellite surface dissolves into copper, sulfide and disulfide ions in the water layer, while under dry condition (e.g. ~RH 2%), this does not occur since little water adsorbs onto NP surfaces. The dissolved sulfide ions may hydrolyze to HS– that is are oxidized by oxygen gas through a two electron reaction of oxygen species involving formation reactive oxygen species as intermediates.[55] Moreover,

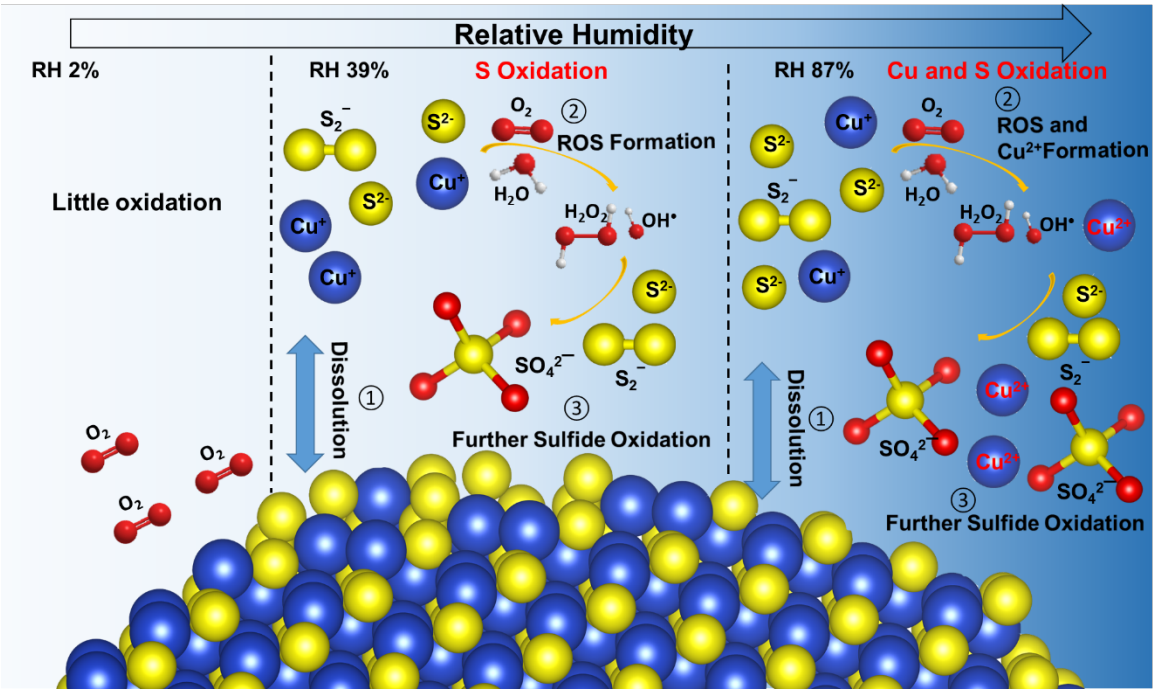

Figure 8. Simplified schematic of the surface during the transformation of CuS nanoparticles under different RH. The transformation processes are composed of three main steps: (1) CuS dissolution in adsorbed water, (2) ROS formation initiated by oxygen in presence of water, (3) further sulfide oxidation by ROS. At RH 87%, Cu^{+} oxidizes to Cu^{2+}.

water also serves as a hard base to stabilize relatively hard acid Cu^{2+} rather than softer Cu^{+} in CuS.[18] Additionally, previous studies of sulfide oxidation show that active metal centers on the surface can promote the formation of hydroxyl radicals.[34, 53, 56, 57, 58] The generation of ROS enhances the oxidation and speeds up these surface transformations. Overall, water is thought to play three key roles: (1) water serves as a medium for the dissolution of CuS; (2) water provides protons for the initial oxidation step by oxygen as shown in the reaction mechanism; (3) water attached to metal centers can dissociate into ROS as an intermediate to accelerate surface oxidation. Adsorbed water is seen to facilitate to the oxidation, so that CuS is oxidized to $CuSO_4$ at high RH i.e. 87%. Interestingly, at RH 39%, there is no Cu^{+} oxidation observed. Therefore, this suggests that Cu_2SO_4 is on the nanoparticle surface and perhaps an intermediate to $CuSO_4$ at higher RH. Taken together he results imply the surface of covellite CuS NPs can be irreversibly transformed in humid environments through this oxidation chemistry.

Conclusions

In summary, the transformation of covellite NP surfaces under ambient conditions at different RHs has been systematically investigated. These results show that the synthesized NP surface is more reactive toward oxygen in the presence of water. High RH increases the oxidation rate and with the formation of $CuSO_4$ formation at 87% RH Interestingly, the transformation of Cu^{+} to Cu^{2+} is not observed at intermediate RH of 39%, while sulfate does form suggesting that Cu_2SO_4 may be an intermediate in the reaction to $CuSO_4$. Adsorbed water is proposed to be a medium for this reaction to occur by favoring the surface dissolution of CuS to the corresponding ions and provide protons to yield ROS by oxygen. The conversion of CuS to $CuSO_4$ found in this study will provide insights and

an understanding of the potential impact this chemistry may have in biological and environmental systems.

Conflicts of interest. There are no conflicts to declare.

Acknowledgements. This work is supported by the National Science Foundation under grant number CHE1606607. XPS was performed at the UC Irvine Materials Research Institute (IMRI) using instrumentation funded in part by the National Science Foundation Major Research Instrumentation Program under grant no. CHE-1338173. HR-TEM was also performed at the UC Irvine Materials Research Institute (IMRI).

References

1. J. Y. Park, S. J. Kim, K. Yim, K. S. Dae, Y. Lee, K. P. Dao, J. S. Park, H. B. Jeong, J. H. Chang, H. K. Seo, C. W. Ahn and J. M. Yuk, *Adv. Sci.*, 2019, **6**, 1900264.
2. P. Thiele, J. Neumann, A. Westphal, R. Ludwig, A.-M. Bonsa, A. Appelhagen, P. Malcher and M. Köckerling, *J. Electrochem. Soc.*, 2017, **164**, A770-A774.
3. H. Wu and W. Chen, *Nanoscale*, 2011, **3**, 5096-5102.
4. H. Wu and W. Chen, *J. Am. Chem. Soc.*, 2011, **133**, 15236-15239.
5. H. Lee, S. W. Yoon, E. J. Kim and J. Park, *Nano Lett.*, 2007, **7**, 778-784.
6. Y. Wu, C. Wadia, W. Ma, B. Sadtler and A. P. Alivisatos, *Nano Lett.*, 2008, **8**, 2551-2555.
7. P. Kar, S. Farsinezhad, X. Zhang and K. Shankar, *Nanoscale*, 2014, **6**, 14305-14318.
8. W. M. B. Roberts and A. S. Buchanan, *Miner. Depos.*, 1971, **6**, 23-33.
9. A. Comin and L. Manna, *Chem. Soc. Rev.*, 2014, **43**, 3957-3975.
10. W. Gao, Y. Sun, M. Cai, Y. Zhao, W. Cao, Z. Liu, G. Cui and B. Tang, *Nat. Commun.*, 2018, **9**, 231.
11. R. P. Brannigan and A. P. Dove, *Biomater. Sci.*, 2017, **5**, 9-21.
12. S. Wang, A. Riedinger, H. Li, C. Fu, H. Liu, L. Li, T. Liu, L. Tan, M. J. Barthel, G. Pugliese, F. De Donato, M. Scotto D'Abbusco, X. Meng, L. Manna, H. Meng and T. Pellegrino, *ACS Nano*, 2015, **9**, 1788-1800.
13. J. P. Gramp, K. Sasaki, J. M. Bigham, O. V. Karnachuk and O. H. Tuovinen, *Geomicrobiol. J.*, 2006, **23**, 613-619.
14. M. Bhagat, J. E. Burgess, A. P. M. Antunes, C. G. Whiteley and J. R. Duncan, *Miner. Eng.*, 2004, **17**, 925-932.
15. L. Legrand Daniel, H. W. Nesbitt and G. M. Bancroft, *Am. Mineral.*, 1998, **83**, 1256.
16. Y. Xie, L. Carbone, C. Nobile, V. Grillo, S. D'Agostino, F. Della Sala, C. Giannini, D. Altamura, C. Oelsner, C. Kryschi and P. D. Cozzoli, *ACS Nano*, 2013, **7**, 7352-7369.
17. T. Wei, Y. Liu, W. Dong, Y. Zhang, C. Huang, Y. Sun, X. Chen and N. Dai, *ACS Appl. Mater. Interfaces*, 2013, **5**, 10473-10477.
18. Y. Xie, A. Riedinger, M. Prato, A. Casu, A. Genovese, P. Guardia, S. Sottini, C. Sangregorio, K. Miszta, S. Ghosh, T. Pellegrino and L. Manna, *J. Am. Chem. Soc.*, 2013, **135**, 17630-17637.

19. J. Ludwig, L. An, B. Pattengale, Q. Kong, X. Zhang, P. Xi and J. Huang, *J. Phys. Chem. Lett.*, 2015, **6**, 2671-2675.
20. U. Shamraiz, R. A. Hussain and A. Badshah, *J. Solid State Chem.*, 2016, **238**, 25-40.
21. A. N. Pham, G. Xing, C. J. Miller and T. D. Waite, *J. Catal.*, 2013, **301**, 54-64.
22. S. Turnbull, B. J. Tabner, D. R. Brown and D. Allsop, *Neurosci. Lett.*, 2003, **336**, 159-162.
23. K. A. C. de Schamphelaere and C. R. Janssen, *Environ. Sci. Technol.*, 2002, **36**, 48-54.
24. M. Grosell, J. Blanchard, K. V. Brix and R. Gerdes, *Aquat. Toxicol.*, 2007, **84**, 162-172.
25. R. B. Jonas, *Appl. Environ. Microbiol.*, 1989, **55**, 43.
26. Z. Yang, H. Li, S. Feng, P. Li, C. Liao, X. Liu, J. Zhao, J. Yang, P.-H. Lee and K. Shih, *Langmuir*, 2018, **34**, 8739-8749.
27. A. M. Jubb and H. C. Allen, *J. Phys. Chem. C.*, 2012, **116**, 9085-9091.
28. K. Kunimatsu, M. G. Samant and H. Seki, *J. Electroanal. Chem.*, 1989, **258**, 163-177.
29. E. A. SECCO, *Can. J. Chem.*, 1987, **66**, 329-336.
30. S. J. Hug, *J. Colloid Interface Sci.*, 1997, **188**, 415-422.
31. A. M. Jubb, D. Verreault, R. Posner, L. J. Criscenti, L. E. Katz and H. C. Allen, *J. Colloid Interface Sci.*, 2013, **400**, 140-146.
32. Z. Su, V. Climent, J. Leitch, V. Zamlynny, J. M. Feliu and J. Lipkowski, *Phys. Chem. Chem. Phys.*, 2010, **12**, 15231-15239.
33. T. Iino, K. Ohashi, K. Inoue, K. Judai, N. Nishi and H. Sekiya, *J. Chem. Phys.*, 2007, **126**, 194302.
34. Y. Li, J. Chen, Y. Chen, C. Zhao, Y. Zhang and B. Ke, *Langmuir*, 2018, **34**, 1941-1952.
35. J. Howeard T. Evans and J. A. Konnert, *Am. Mineral.*, 1976, **61**, 996-1000.
36. S. W. Goh, A. N. Buckley and R. N. Lamb, *Miner. Eng.*, 2006, **19**, 204-208.
37. W. Liang and M. H. Whangbo, *Solid State Commun.*, 1993, **85**, 405-408.
38. N. J. Freymeyer, P. D. Cunningham, E. C. Jones, B. J. Golden, A. M. Wiltrout and K. E. Plass, *Crystal Growth & Design*, 2013, **13**, 4059-4065.
39. S.-h. Saito, H. Kishi, K. Nié, H. Nakamaru, F. Wagatsuma and T. Shinohara, *Phys. Rev. B*, 1997, **55**, 14527-14535.
40. G. W. Luther, S. M. Theberge, T. F. Rozan, D. Rickard, C. C. Rowlands and A. Oldroyd, *Environ. Sci. Technol.*, 2002, **36**, 394-402.
41. R. A. D. Pattrick, J. F. W. Mosselmans, J. M. Charnock, K. E. R. England, G. R. Helz, C. D. Garner and D. J. Vaughan, *Geochim. Cosmochim. Acta*, 1997, **61**, 2023-2036.
42. I. I. Mazin, *Phys. Rev. B*, 2012, **85**, 115133.
43. P. Kumar, R. Nagarajan and R. Sarangi, *J. Mater. Chem.C*, 2013, **1**, 2448-2454.
44. S. W. Goh, A. N. Buckley, R. N. Lamb, R. A. Rosenberg and D. Moran, *Geochim. Cosmochim. Acta*, 2006, **70**, 2210-2228.
45. R. R. Gainov, A. V. Dooglav, I. N. Pen'kov, I. R. Mukhamedshin, N. N. Mozgova, I. A. Evlampiev and I. A. Bryzgalov, *Phys. Rev. B*, 2009, **79**, 075115.
46. R. P. Vasquez, *Surface Science Spectra*, 1998, **5**, 279-284.
47. R. V. Siriwardane and J. A. Poston, *Appl. Surf. Sci.*, 1990, **45**, 131-139.
48. C. Malitesta, D. Centonze, L. Sabbatini, P. G. Zambonin, L. P. Bicelli and S. Maffi, *J. Mater. Chem.*, 1991, **1**, 259-263.
49. R. S. C. Smart, W. M. Skinner and A. R. Gerson, *Surf. Interface Anal.*, 1999, **28**, 101-105.
50. M. C. Biesinger, *Surf. Interface Anal.*, 2017, **49**, 1325-1334.
51. V. Hayez, A. Franquet, A. Hubin and H. Terryn, *Surf. Interface Anal.*, 2004, **36**, 876-879.
52. V. B. Llorente, V. M. Dzhagan, N. Gaponik, R. A. Iglesias, D. R. T. Zahn and V. Lesnyak, *J. Phys. Chem. C.*, 2017, **121**, 18244-18253.
53. Z. Wei, Y. Li, H. Gao, Y. Zhu, G. Qian and J. Yao, *Appl. Surf. Sci.*, 2019, **492**, 89-98.
54. R. Cai, Y. Kubota and A. Fujishima, *J. Catal.*, 2003, **219**, 214-218.
55. G. W. Luther, *Aquat. Geochem.*, 2010, **16**, 395-420.

56. M. J. Borda, A. R. Elsetinow, D. R. Strongin and M. A. Schoonen, *Geochim. Cosmochim. Acta*, 2003, **67**, 935-939.
57. P. Zhang, S. Yuan and P. Liao, *Geochim. Cosmochim. Acta*, 2016, **172**, 444-457.
58. C. R. Usher, K. W. Paul, J. Narayansamy, J. D. Kubicki, D. L. Sparks, M. A. A. Schoonen and D. R. Strongin, *Environ. Sci. Technol.*, 2005, **39**, 7576-7584.

TOC